Mesoscale Predictability of Terrain Induced Flows

Dale R. Durran
University of Washington
Dept. of Atmospheric Sciences
Box 351640
Seattle, WA 98195
phone: (206) 543-7440 fax: (206) 543-0308 email: durrand@atmos.washington.edu

Grant Number: N00014-06-1-0827

LONG-TERM GOALS

Allow users of high-resolution mesoscale weather forecasts to understand and assess the likelihood that fine-scale features appearing in the forecast will actually verify. Our results will inform efforts to apply ensemble forecast methodologies to very small-scale weather events.

OBJECTIVES

We seek to evaluate the predictability of downslope wind events as forecast by the Navy's COAMPS model. Since terrain-induced mesoscale phenomena have long been regarded as likely to be among the most predictable mesoscale disturbances, this work may suggest an upper limit on the predictability of a wide range of mesoscale phenomena.

APPROACH

The Terrain-Induced Rotor Experiment (TREX) took place from 1 March – 30 April 2006 in and surrounding the Owens valley of California and the adjacent Sierra Nevada Mountains (Fig. 1b). During the TREX field campaign a large observational network was deployed to document, among other things, the temporal evolution of downslope winds, topographically generated mountain waves, and terrain-induced rotors.

We will use several cases selected from the TREX field campaign to study the predictive capability of mesoscale models, in particular, the ability of modern, high-resolution mesoscale models to predict downslope winds and mountain waves.

Recently developed ensemble techniques, such as ensemble Kalman filters (EnKF), will be used in this multi-scale predictability problem. In particular, we use a 70-member ensemble, generated with a square-root EnKF (Whitaker and Hamill, 2002) on three computational domains (27, 9, and 3 km) centered on the Owens valley and Sierra Nevada Mountains (Fig. 1). The EnKF is an ensemble-based data assimilation method, which under suitable assumptions provides an optimal combination of observations and background estimates of the atmosphere (Hamill, 2006). The EnKF takes into account both observational error and the error in a background forecast to give an expected analysis of the atmosphere along with the expected variability in the analysis for the particular atmospheric conditions at the time of the analysis. We will use the EnKF to assimilate real observations every 6 hours during periods of mountain wave and downslope wind activity. The 70 ensemble members will

Report Documentation Page

Form Approved
OMB No. 0704-0188

1. REPORT DATE	2. REPORT TYPE	3. DATES COVERED
30 SEP 2007	**Annual**	**00-00-2007 to 00-00-2007**

4. TITLE AND SUBTITLE	5a. CONTRACT NUMBER
Mesoscale Predictability Of Terrain Induced Flows	5b. GRANT NUMBER
	5c. PROGRAM ELEMENT NUMBER
6. AUTHOR(S)	5d. PROJECT NUMBER
	5e. TASK NUMBER
	5f. WORK UNIT NUMBER
7. PERFORMING ORGANIZATION NAME(S) AND ADDRESS(ES) **University of Washington,Dept. of Atmospheric Sciences,Box 351640,Seattle,WA,98195**	8. PERFORMING ORGANIZATION REPORT NUMBER
9. SPONSORING/MONITORING AGENCY NAME(S) AND ADDRESS(ES)	10. SPONSOR/MONITOR'S ACRONYM(S)
	11. SPONSOR/MONITOR'S REPORT NUMBER(S)

12. DISTRIBUTION/AVAILABILITY STATEMENT
Approved for public release; distribution unlimited

13. SUPPLEMENTARY NOTES
code 1 only

14. ABSTRACT
Allow users of high-resolution mesoscale weather forecasts to understand and assess the likelihood that fine-scale features appearing in the forecast will actually verify. Our results will inform efforts to apply ensemble forecast methodologies to very small-scale weather events.

15. SUBJECT TERMS

16. SECURITY CLASSIFICATION OF:			17. LIMITATION OF ABSTRACT	18. NUMBER OF PAGES	19a. NAME OF RESPONSIBLE PERSON
a. REPORT	b. ABSTRACT	c. THIS PAGE			
unclassified	**unclassified**	**unclassified**	**Same as Report (SAR)**	**8**	

then be integrated forward with the COAMPS mesoscale model. Boundary conditions on the 27 km domain are provided by NOGAPS and perturbed for each member with the fixed covariance method described in (Torn et. al., 2006).

Individuals working on this project include the PI Dale Durran and one graduate student, Alex Reinecke.

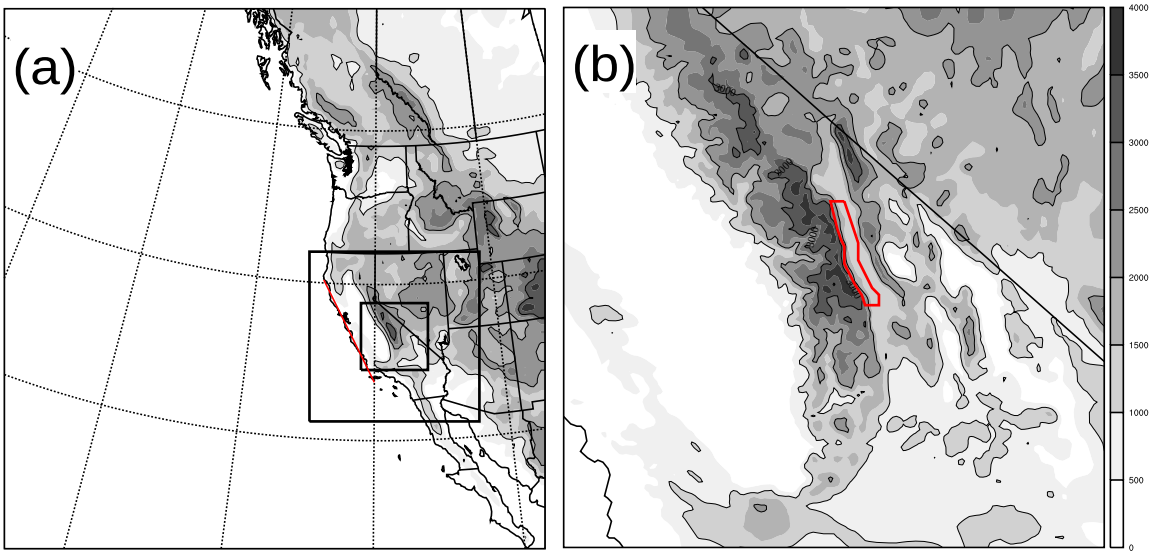

Figure 1: Topography and location of the (a) 27 km, 9 km and 3 km domains. The red line along the California coast indicates the location of the cross-sections in Fig. 4. (b) Topography of the 3 km innermost mesh. The red box indicates the horizontal region throughout which the wind speed metric is calculated.

WORK COMPLETED

In order to properly calibrate the ensemble, a reanalysis of the entire field campaign was completed on the coarse, 27 km domain (Fig. 1a). For the reanalysis the standard radiosonde network, ACARS data, cloud-track winds, and surface ASOS data was assimilated every 6 hours. The reanalysis is of interest in its own right since it provides probabilistic information about the synoptic-state during the entire TREX period. The reanalysis data also provides initial conditions in which to nest the ensemble to higher resolutions (9 and 3 km grid spacing) for specific periods of interest.

The ensemble has been nested to higher resolution for 8 specific cases during the TREX field campaign. In addition to the standard synoptic observations, additional observations collected during TREX are assimilated on the higher-resolution domains. The effect of these observations on the analysis will be discussed below. Results for two events will be presented below: IOP 6, a 12-hour forecast initialized on 18 UTC 25 March, 2006 and IOP 13, a 12-hour forecast initialized at 00 UTC 17 April, 2006. For both of these events, high-resolution forecasts were made for several assimilation cycles prior to the period of interest so that mesoscale structure was present in the analysis.

RESULTS

The ensemble mean downslope wind speed, calculated as the component of wind perpendicular to the Sierra crest and averaged over a 350 m deep box in the Owens Valley (red box in Fig. 1a) is shown by the dotted line for IOP 6 and IOP 13 in Fig. 2a and 2b, respectively. Both events show a maximum in the mean wind speed at hour 7. While the ensemble mean shows the peak in the wind storm at this time, the individual members have considerable spread. The solid and dashed lines show the time evolution of the strongest and weakest 10 members (ranked at hour 7). The difference in wind speed between the strongest and weakest 10 members is roughly 35 m/s for both IOP 6 and 13. *Such large differences in downslope wind speeds indicate that expected synoptic variability can produce a very wide range of responses on the mesoscale.*

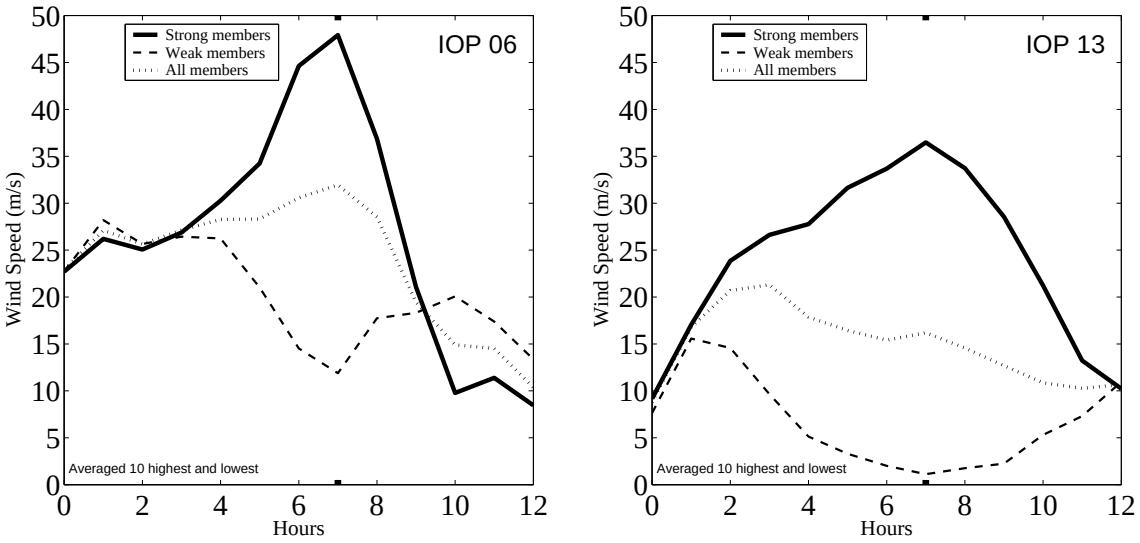

Figure 2: Time series plot of the IOP 6 and IOP 13 Sierra-perpendicular downslope wind speeds calculated in the lee-side metric box for the strongest 10, weakest 10, and ensemble mean. The downslope wind speeds are ranked at forecast hour 7 for both IOP 6 and IOP 13.

How different are the synoptic-scale environments responsible for the strong and weak downslope wind storms? Figures 3 and 4 show cross-sections of the Sierra-perpendicular component of the wind and isentropes of potential temperature (θ) on the 9 km domain along the California coast (Fig. 1a) for IOP 6 and IOP 13 respectively. The times of the cross-sections are 4 and 2 hours prior to the peak windstorm for IOP 6 and 13 respectively; and correspond to the time when back trajectories, launched at the time of maximum wind (hour 7) from the crest of the Sierra, reach the California coast. Figure 3 shows upstream cross-sections averaged over the strongest (panel a) and weakest (panel b) 10 members in IOP 6. Both the strong and weak cases have an upper-level front extending into the lower troposphere and both have a jet of Sierra-perpendicular wind exceeding 45 m/s. The upstream differences are very small and would present significant challenges for a forecaster trying to distinguish between the strong and weak events.

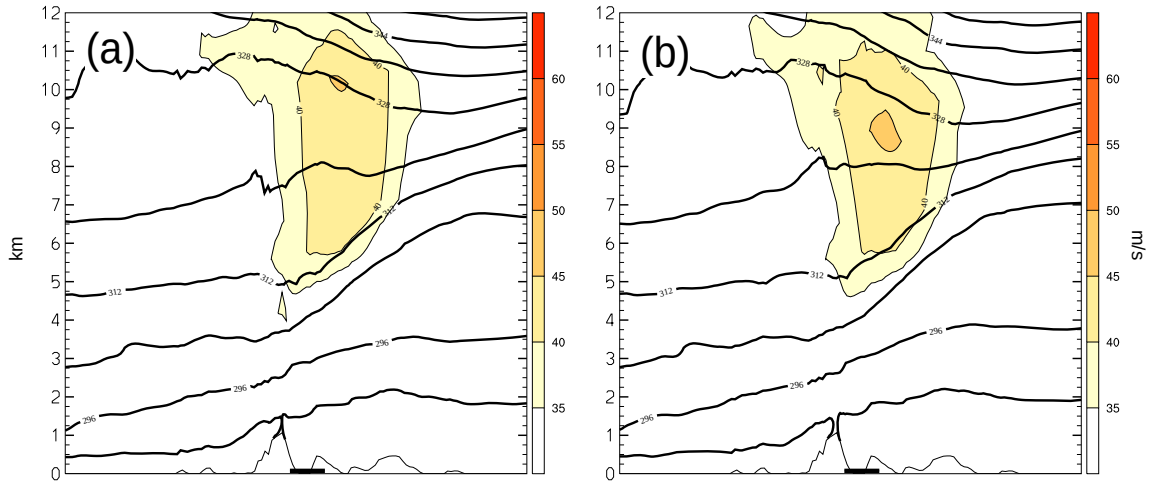

Figure 3: IOP 6 upstream cross-section along the California coast on the 9 km domain of the Sierra perpendicular winds (ci=5 m/s) and θ contours (ci=8 K) for the (a) strongest 10 downslope wind members and (b) weakest 10 downslope wind members.

For IOP 13 the differences in the upstream Sierra-perpendicular winds and θ fields between the strongest and weakest events are considerably greater than for IOP 6. Figures 4a and 4b show the cross-section of Sierra-perpendicular winds and θ averaged over the strongest and weakest 10 downslope wind events. An upper-level front is present in both the strong and weak cases, but the front and the associated jet max are both significantly stronger in the strong-wind case. In particular, the maximum wind speeds in the jet are roughly 10 m/s stronger for the strong cases than for the weak ones. (In contrast, the strongest events in IOP 6 were associated with the cases with the slightly weaker upstream jet.) The rms differences between the strong and weak events in both the winds and the θ fields, averaged over the plane of the upstream cross-section, are roughly twice as large in IOP 13 as for IOP 6, these differences are still within the range of uncertainty inherent in the data assimilation process, and it would be unwise to assume that a single deterministic forecast could confidently predict the downslope wind response.

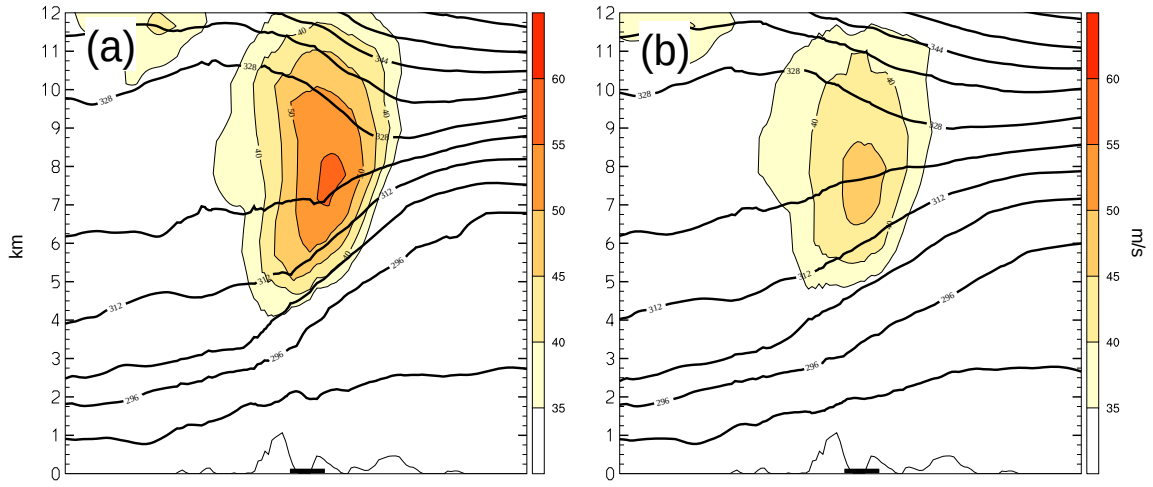

Figure 4: IOP 13 upstream cross-section along the California coast on the 9 km domain of the Sierra perpendicular winds (ci=5 m/s) and θ contours (ci=8 K) for the (a) strongest 10 downslope wind members and (b) weakest 10 downslope wind members.

Figure 5 shows one way of displaying the uncertainty in the forecast downslope winds revealed by the various ensemble members. Looking at the problem from a forecasting point of view one can ask the question; what is the probability that the ensemble mean downslope wind speed will be over-forecast or under-forecast? Figure 5 answers this by estimating the probability that the 7-hour forecast downslope winds will exceed various thresholds. This probability is calculated by binning the downslope wind speed averaged over the box (Fig. 1b) into 1 m/s bins, dividing the number of ensemble members in each bin by the total size of the ensemble, and then subtracting the cumulative sums from 1. The ensemble mean of all 70 members is indicated by the red line for both IOP 6 (panel a) and IOP 13 (panel b). Thus, according to Fig. 5a, we estimate that in IOP 6 there is a 100% chance that the downslope wind speed will exceed 5 m/s, a 56% chance that the winds will exceed the ensemble mean of 32 m/s, and a 9% chance that the winds will exceed 47 m/s. Looking at this from another point of view, if there is a large amount of area below the black curve and right of the red line, then there is a high chance a forecast of the ensemble mean will be an under-forecast. If there is a large area above the curve and to the left of the red line then there is a high chance that the ensemble mean forecast is an over-forecast. Figure 5 indicates that both IOP 6 and IOP 13 have a large amount of spread about the ensemble mean and that an even the ensemble mean forecast has a high likelihood of being in significant error. That is, both IOP 6 and IOP 13 have a low level of predictability. Other IOP's such as IOP 4 (not shown) suggest that there is often a greater chance of over-predicting the wind storm than under-predicting it.

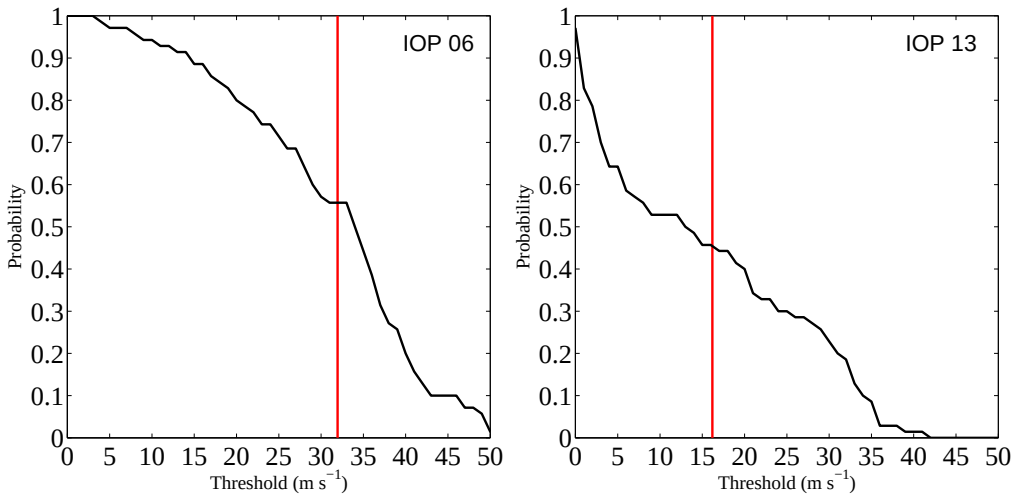

Figure 5: The probability that the Sierra perpendicular downslope wind speeds will reach a threshold value at forecast hour 7 for IOP 6 and IOP 13. The red line indicates the ensemble mean.

While the use of an ensemble to study the predictability of mesoscale flows is of interest in its own right, the EnKF has the potential to be a powerful tool in mesoscale data assimilation. Topographically driven flows provide a unique opportunity to study data assimilation on the mesoscale, since the features of interest are often fixed to the topography and an intelligently placed fixed observational network can routinely observe the phenomenon. A pertinent question is: can surface observations of downslope winds provide meaningful improvements in the representation of upper-level mesoscale features, such as topographically generated gravity-waves? The EnKF is of particular interest for data assimilation in topographically driven mesoscale flows because of the highly flow-dependent nature of background-error covariance. More traditional methods of data assimilation such as 3D-Var or MVOI have externally specified background-error covariance, which have no knowledge of mesoscale flow features such as downslope wind and mountain waves. At the center of the EnKF is the Kalman gain, which represents the increment in the model variable about the ensemble mean that would be produced by a unit-amplitude increase relative to the ensemble mean at some specific data point.

Figure 6 shows the Kalman gain for the IOP 6 analysis due to an observation of a 1 m/s increase in the Sierra-perpendicular wind speed at a point 10 m AGL indicated by the dot in the Owens Valley in panel a. The horizontal field of the gain in the 100 m AGL Sierra-perpendicular wind speed is shown in Fig. 6a. Positive values of the Kalman gain are spread along the lee-slope of the Sierra, indicating that a positive observation increment of the low-level downslope wind will increase the winds along the lee-slopes in a manner suggestive of a stronger downslope wind event. The increase in wind speed is not distributed across the width of the valley as it might be by some assimilation method based on a "radius of influence." Looking along a Sierra-perpendicular vertical cross-section through the observation point (Fig. 6b), the positive Kalman gain in the horizontal wind field extends upwards roughly 1 km. Above this region there is a weakly negative area of Kalman gain indicating that a positive increment in downslope winds will weaken the winds aloft. The Kalman gain in the Sierra-perpendicular wind field is entirely consistent with mountain-wave/downslope wind theory. Stronger downslope winds are associated with stronger mountain-waves, which have weaker wind speeds aloft. Also of note is the Kalman gain in the vertical velocity field (Fig. 6b) which shows that a positive

increment in downslope wind speeds produces a positive/negative couplet aloft that appears shift and strengthen the vertical velocity within the mountain wave.

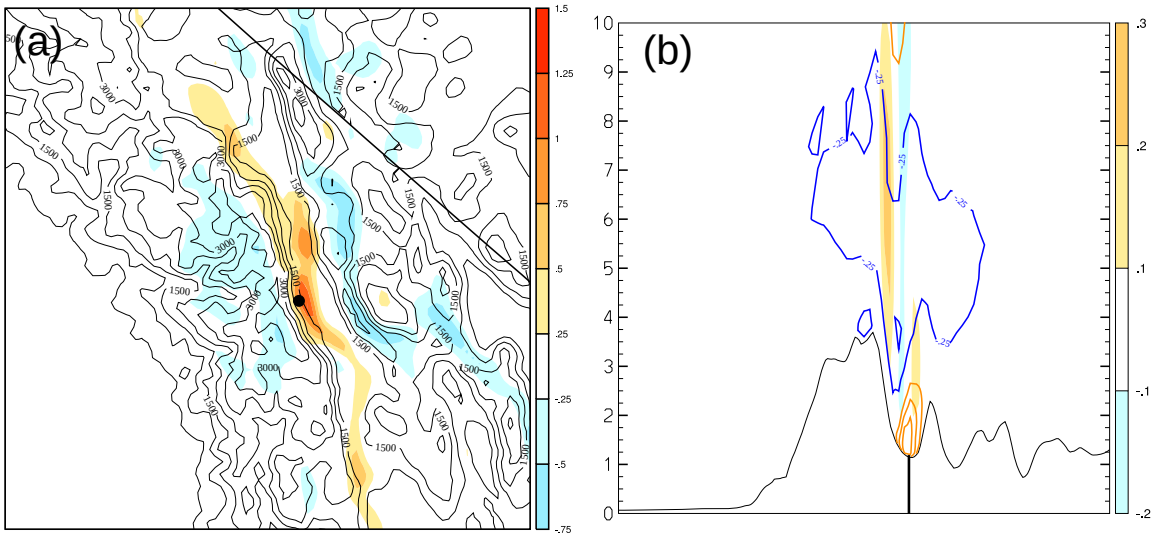

Figure 6: Kalman gain between the Sierra perpendicular wind at the black dot and the (a) Sierra perpendicular wind at 100 m AGL (ci=0.25) and (b) the vertical velocity (colored; ci=0.1) and Sierra perpendicular wind (ci=0.25; zero contour omitted) in a vertical cross-section.

IMPACT/APPLICATIONS

With ever increasing computer power, real-time mesoscale models are producing mesoscale forecasts at higher and higher resolutions. The need to understand the predictive limit of these models at such high resolution is therefore necessary. Additionally, higher resolution mesoscale ensemble systems are also on the near horizon. Ensemble data assimilation systems, such as an EnKF, are powerful tools to incorporate forecast uncertainty and observational uncertainty in order to provide the best possible initial model conditions. Understanding to what extent these techniques can be applied on mesoscale features will be of great importance when such high-resolution systems come on-line in real-time.

RELATED PROJECTS

There are no related projects.

REFERENCES

Hamill, T. M., 2006: Ensemble-based atmospheric data assimilation: A tutorial. Predictability of weather and climate, T. Palmer and R. Hagedorn, Eds., Cambridge University Press. 124–156.

Torn, R. D., G. J. Hakim, and C. Snyder, 2006: Boundary conditions for a limited-area ensemble Kalman filter. Mon. Wea. Rev., 134, 2490–2502.

Whitaker, J. S. and T. M. Hamill, 2002: Ensemble data assimilation without perturbed observations. Mon. Wea. Rev., 130, 1913–1924.

HONORS/AWARDS

Alex Reinecke, University of Washington. "Best oral presentation by a young scientist", 29th International Conference on Alpine Meteorology, Chambery, France.